

Article

# An Effective Label-Free Electrochemical Aptasensor Based on Gold Nanoparticles for Gluten Detection

Rossella Svigelj <sup>\*</sup>, Ivan Zuliani, Cristian Grazioli, Nicolò Dossi and Rosanna Toniolo <sup>\*</sup>

Department of Agrifood, Environmental and Animal Science, University of Udine, Via Cotonificio 108, 33100 Udine, Italy; zuliani.ivan@spes.uniud.it (I.Z.); cristian.grazioli@uniud.it (C.G.); nicolo.dossi@uniud.it (N.D.)

<sup>\*</sup> Correspondence: rossella.svigelj@uniud.it (R.S.); rosanna.toniolo@uniud.it (R.T.)

**Abstract:** Nanomaterials can be used to modify electrodes and improve the conductivity and the performance of electrochemical sensors. Among various nanomaterials, gold-based nanostructures have been used as an anchoring platform for the functionalization of biosensor surfaces. One of the main advantages of using gold for the modification of electrodes is its great affinity for thiol-containing molecules, such as proteins, forming a strong Au-S bond. In this work, we present an impedimetric biosensor based on gold nanoparticles and a truncated aptamer for the quantification of gluten in hydrolyzed matrices such as beer and soy sauce. A good relationship between the  $R_{ct}$  values and PWG-Gliadin concentration was found in the range between 0.1–1 mg L<sup>-1</sup> of gliadin (corresponding to 0.2–2 mg L<sup>-1</sup> of gluten) with a limit of detection of 0.05 mg L<sup>-1</sup> of gliadin (corresponding to 0.1 mg L<sup>-1</sup> of gluten). The label-free assay was also successfully applied for the determination of real food samples.

**Keywords:** aptamers; aptasensor; beer; electrochemical impedance spectroscopy; food allergen; gluten; gold nanoparticles; impedimetric biosensor; soy sauce



**Citation:** Svigelj, R.; Zuliani, I.; Grazioli, C.; Dossi, N.; Toniolo, R. An Effective Label-Free Electrochemical Aptasensor Based on Gold Nanoparticles for Gluten Detection. *Nanomaterials* **2022**, *12*, 987. <https://doi.org/10.3390/nano12060987>

Academic Editor: Baizeng Fang

Received: 11 February 2022

Accepted: 15 March 2022

Published: 17 March 2022

**Publisher's Note:** MDPI stays neutral with regard to jurisdictional claims in published maps and institutional affiliations.



**Copyright:** © 2022 by the authors. Licensee MDPI, Basel, Switzerland. This article is an open access article distributed under the terms and conditions of the Creative Commons Attribution (CC BY) license (<https://creativecommons.org/licenses/by/4.0/>).

## 1. Introduction

Nanomaterials have been applied in different fields such as electrochemistry [1–3], medicine [4,5], engineering [6], and many others [7,8]. The physical and chemical properties of nanomaterials change depending on their composition, shape, and size, and thanks to their tunable characteristics, they are increasingly used to improve the performance of electrochemical sensors [9–11]. In addition, their high surface area allows the easy immobilization of biomolecules such as proteins and aptamers; hence, applications based on nanoparticles in biosensor development are growing [12–15].

Among various metallic nanomaterials, gold-based nanostructures have been used as an anchoring platform for the functionalization of biosensor surfaces [16]. One of the main advantages in the use of gold is its biocompatibility and the strong bond that can be formed between molecules containing thiols, such as proteins, and the surface of gold nanomaterials [17]. Moreover, it is possible to use gold nanomaterials with different shapes such as nanoparticles, nanorods, nanoshells, and nanostars [18]. Gold nanoparticles (AuNPs) present a high surface-to-volume ratio, high surface energy, and the ability to improve electron transfer between redox species and the electrode surface. Hence thanks to their characteristics, the use of nanomaterials for the construction of electrochemical biosensors enhances the analytical performance when compared to other biosensor designs [19,20].

Highly sensitive nanobiosensors make possible the detection of analytes when they are present in very low concentrations, such as food allergens [21,22]. According to the Food and Drug Administration (FDA), about 90% of food allergy cases are triggered by milk, eggs, fish, shellfish, tree nuts, wheat, peanuts, and soy [23]. So far, a diet without food containing allergenic ingredients is the only strategy that avoids allergies in hypersensitive

individuals. Gluten is identified as one of the eight major food allergens. Accordingly, the European Union took specific action to protect the health of consumers suffering from coeliac disease, defining that the term “gluten-free” is allowed in foods with a gluten content of less than 20 mg/kg, and that “very low gluten” refers only to products with a quantity of gluten between 20 mg/kg and 100 mg/kg. In predisposed individuals, the intake of gluten causes coeliac disease, which is a chronic condition that involves the immune system and compromises the intestinal villi [24,25]. After ingestion, gluten is partially broken by gastrointestinal enzymes into peptides [26]. These peptides are rich in proline and glutamine, and this characteristic makes them resistant to proteolysis in the human gut [27]. Some of these peptides can cause an immune-toxic response, which may evolve in local tissue damage [28]. These peptides can be found in some fermented foods, such as beer. From an analytical point of view, these types of real matrices are difficult to analyze because the target is small compared to the non-hydrolyzed protein [29,30]. For this reason, label-free assays are important. Unlike the sandwich assays, in which the protein must be present in an intact form, with a label-free approach, only one recognition element is used. Hence, it is possible to carry out a precise quantification of gluten even in matrices where the protein is in the hydrolyzed form. Moreover, the simplicity and rapidity of the detection make label-free assays of increasing interest.

In recent years, various approaches have been proposed for the quantification of gluten based on aptamers [31,32], among them various sandwich assays [33,34] and some label-free [35,36]. However, the label-free assays proposed so far have not been very effective in the determination of gluten at low concentrations, a very important factor for the population of people sensitive even to very low concentrations of gluten. For this purpose, in this work, we present a rapid platform based on electrochemical impedance spectroscopy (EIS) for the quantification of gluten in hydrolyzed matrices such as beer and soy sauce. The proposed biosensor uses AuNPs as an anchoring platform and a truncated aptamer with a high affinity for the analyte [33]. The ability of gold nanoparticles to provide a stable immobilization of biomolecules maintaining their bioactivity will be exploited. Moreover, the benefits of using a nanostructured gold surface instead of a gold surface are an improved electron transfer property and increased surface area for the subsequent modifications. In the literature, some studies have already reported the successful development of biosensors on screen-printed carbon electrodes modified with AuNPs for the determination of analytes present in low concentrations [37,38].

## 2. Materials and Methods

### 2.1. Chemicals and Reagents

5'-tagged (biotin) truncated aptamer Gli4-T (sequence: CTA CAC ATG TCT GAA TGC C) was obtained HPLC-purified from Sigma Aldrich (Milan, Italy). Bovine serum albumin (BSA), sorbitol, and biotin were purchased from Sigma Aldrich (Milan, Italy). Streptavidin and Horseradish peroxidase (HRP) conjugated with streptavidin were purchased from Merck (Milan, Italy). Tetrachloroauric acid was purchased by J.M. Chemicals (London, UK). PWG-Gliadin was kindly provided by the Prolamine Working Group (Freising, Germany). Ultrapure water ( $R > 18 \text{ M}\Omega$ ) was obtained by means of an Elga Purelab flex 4 system (Veolia Water Technologies, Milan, Italy) and used for the preparation of buffer solutions.

### 2.2. Apparatus

Screen-printed carbon electrodes were purchased by Dropsens (Metrohm, Milan, Italy). All voltammetric and impedance measurements were performed using an Autolab PGSTAT204 potentiostat (Metrohm, Milan, Italy) managed by Nova software version 3.2 and connected to the SPCE by means of a CAC connector cable from Dropsens (Metrohm, Milan, Italy).

Morphological and structural properties of AuNPs were investigated by Field Emission Scanning Electron Microscopy (FE-SEM) performed by JEOL model JSM-7610FPlus.

### 2.3. Electrochemical Impedance Spectroscopy (EIS) Measurements

The electrochemical impedance spectroscopy measurements were conducted using the redox probe  $[\text{Fe}(\text{CN})_6]^{4-}/[\text{Fe}(\text{CN})_6]^{3-}$  2 mM each, KCl 3 mM in PBS. The applied potential was 0.115 V (half-wave potential of the redox pair), while the frequency was varied in the range from 10,000 Hz to 0.01 Hz, with an amplitude of 0.005 V. The resistance to charge transfer ( $R_{ct}$ ) was calculated using NOVA software.

All the measurements were carried out at room temperature on an SPCE. The same measurement procedure was also used in the analysis of real samples.

### 2.4. Modification Procedure of SPCE with AuNPs

In order to increase the sensitivity of the impedimetric biosensor, two strategies exploiting gold particles were evaluated. The first strategy involved the modification of the surface by drop-casting. For this purpose, 20  $\mu\text{L}$  of a 5 mM AuNPs aqueous solution, previously synthesized in our laboratory as reported in the literature [39], were drop-casted on the electrode surface and allowed to evaporate. Briefly, the AuNPs were synthesized as follows: 1 mM  $\text{HAuCl}_4$  solution was put to reflux under stirring, then a 38 mM sodium citrate solution was quickly added, the color of the solution changed from yellow to deep red. The system was let on reflux for 20 min, and after that time, the solution was cooled down to room temperature under stirring.

The second strategy involved the electrochemical deposition of AuNPs. In this approach, two parameters are crucial to controlling the size and shape of NPs: the potential applied and the time of deposition. First, we conducted a voltammetric investigation, as reported in Figure 1. Then, to identify the best conditions, we performed the deposition of AuNPs at different potentials of 0.6 V, 0.4 V, and finally, 0.18 V. As can be seen from Figure S1, the measurements of impedance conducted on the modified SPCE indicate that the surface with the least resistance at the charge transfer is that modified at 0.18 V, in agreement with the literature [10,39].

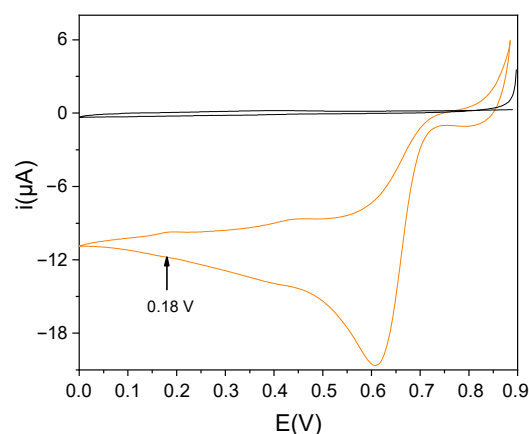


**Figure 1.** Cyclic voltammetry recorded on SPCE for a 1 mM solution of  $\text{HAuCl}_4$  in 0.5 M  $\text{H}_2\text{SO}_4$  (orange line). Background cyclic voltammetry recorded in 0.5 M  $\text{H}_2\text{SO}_4$  (black line). The arrow indicates the potential chosen for the electrochemical generation of AuNPs.

Secondly, we studied the deposition time, ensuring the best performance. For this purpose, chronoamperometry measurements were carried out at different times (10, 20, 30, 40, 50, 60 s), and as can be seen from Figure S2, the amount of charge expended during the deposition increases with time. Then, EIS measurements for each modification at different times were performed. Figure S3 shows that after 50 s, there is no improvement from the point of view of charge transfer. In the light of these results, all the subsequent experimentation was conducted by modifying the electrodes as follows: 40  $\mu\text{L}$  of a 1 mM solution of  $\text{HAuCl}_4$  in 0.5 M  $\text{H}_2\text{SO}_4$  was placed on the electrode surface, and 0.18 V was applied for 50 s.

### 2.5. Biosensor Assembly

First, the surface of the working electrode of the SPCE was washed with 500  $\mu\text{L}$  of ethanol and dried with air. Subsequently, the electrochemical deposition of gold nanoparticles (AuNPs) was carried out by drop-casting 40  $\mu\text{L}$  of a solution of tetrachloroauric acid ( $\text{HAuCl}_4$ ) 1 mM in 0.5 M  $\text{H}_2\text{SO}_4$  and applying 0.18 V for 50 s. Next, the surface of the SPCE was washed three times with phosphate buffer solution (PBS) pH 7.4 and dried with air. A total of 10  $\mu\text{L}$  of streptavidin 1 mg  $\text{mL}^{-1}$  were immobilized on the bare carbon working electrode by adsorption at 4  $^\circ\text{C}$  overnight; then, the surface was blocked with 20  $\mu\text{L}$  of BSA 1% and sorbitol 6% in PBS for 30 min. Then, the SPCE was again washed and covered with 20  $\mu\text{L}$  1  $\mu\text{M}$  solution of Gli4T-biotin in PBS for 30 min. Finally, the surface was covered with 20  $\mu\text{L}$  of 0.5  $\mu\text{M}$  biotin in PBS for 10 min. Figure 2 shows the functionalization protocol of the modified SPCE with electrogenerated AuNPs, in which, in the end, the presence or absence of PWG-Gliadin was detected using the redox probe  $[\text{Fe}(\text{CN})_6]^{3-}/[\text{Fe}(\text{CN})_6]^{4-}$ .

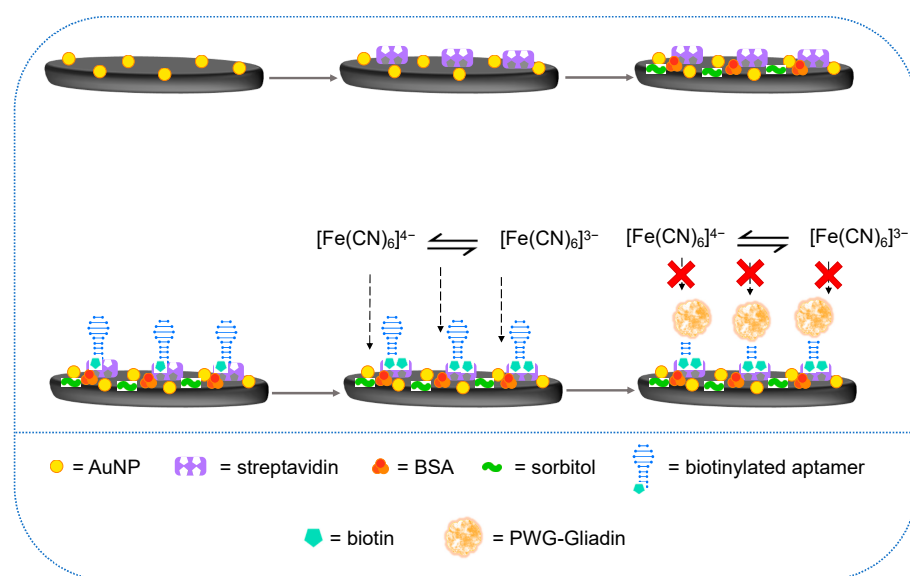


**Figure 2.** Schematic representation of the aptasensor design and its working principle: after the electrochemical deposition of AuNPs streptavidin was immobilized on the working electrode, then a solution of BSA and sorbitol was used to block the surface; subsequently, the biotinylated aptamer was immobilized, and after a final step of blocking with biotin, the sensor was ready to use. The redox probe  $[\text{Fe}(\text{CN})_6]^{3-}/[\text{Fe}(\text{CN})_6]^{4-}$  was employed to evaluate the presence or absence of PWG-Gliadin.

### 2.6. Gliadin Detection

20  $\mu\text{L}$  of the solutions at different concentrations of PWG-Gliadin in buffer solution (20 mM Tris-HCl, 100 mM NaCl and 2 mM  $\text{MgCl}_2$ ) were deposited on the working electrodes of the previously modified SPCEs.

After half an hour of incubation, the surface of the WE of the SPCE was rinsed three times with 250  $\mu\text{L}$  aliquots of buffer and dried with air. Subsequently, 40  $\mu\text{L}$  of a PBS solution containing 3 mM KCl, 2 mM  $[\text{Fe}(\text{CN})_6]^{3-}$  and 2 mM  $[\text{Fe}(\text{CN})_6]^{4-}$  were added on the SPCE, and immediately the impedance measurement was performed. The same procedure was also used in the analysis of real samples after dilution and enrichment with known quantities of PWG-Gliadin.

## 3. Results and Discussion

### 3.1. Electrochemical Characterization of SPCE Modified with AuNPs

In order to evaluate the efficiency of the two modification strategies, the SPCEs were analyzed by cyclic voltammetry and EIS. The results are shown in Figure 3. The

voltammetric behavior of the SPCE modified with electrogenerated AuNPs confirms the ability of gold nanoparticles to enhance conductivity. In fact, Figure 3B shows that in all spectra, a semicircular portion is predominant and how both modification strategies lead to a reduction of the related radius. However, by comparing the Nyquist plots obtained on the gold-modified SPCEs, it is possible to see how the electrochemical deposition of AuNPs leads to a lower charge transfer resistance, confirming that this approach is more effective than the modification carried out by drop-casting. To attain more insight concerning these behaviors, a SEM characterization of both modified screen-printed electrodes was performed.

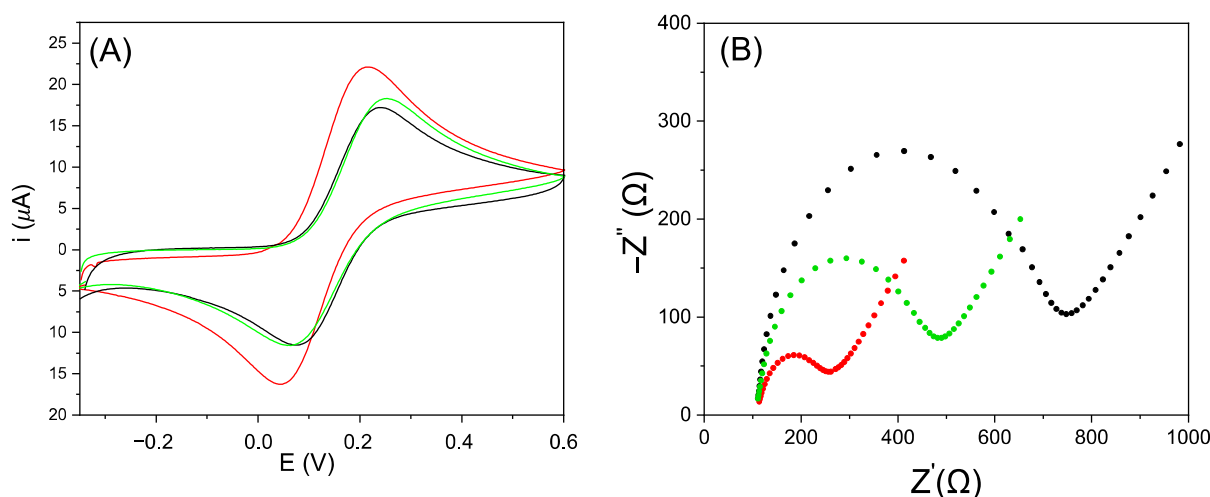


**Figure 3.** (A) Cyclic voltammograms of ferrocyanide 1 mM in KCl 100 mM on the bare screen-printed carbon electrode (SPCE) in black, on the SPCE modified with AuNPs by drop-casting in green and on the SPCE modified with electrogenerated AuNPs in red. (B) Nyquist plots recorded using the redox probe  $[\text{Fe}(\text{CN})_6]^{4-}/[\text{Fe}(\text{CN})_6]^{3-}$  2 mM each, KCl 3 mM in PBS at unmodified SPCE (black,  $R_{\text{ct}} = 614.44 \Omega$ ), modified with AuNPs deposited by drop-casting (green,  $R_{\text{ct}} = 372.85 \Omega$ ) and modified with electrogenerated AuNPs (red,  $R_{\text{ct}} = 172.95 \Omega$ ).

### 3.2. SEM Characterization of Modified SPCE

The morphology of SPCEs modified with AuNPs was investigated by a Field Emission Scanning Electron Microscopy. Figure 4A,B shows the SEM images of an SPCE before and after the modification with electrogenerated AuNPs. Instead, in Figure 4C,D, the morphology and size of the AuNPs can be seen in more detail. It is possible to observe that the carbon electrode surface is evenly covered by spherical AuNPs. Conversely, the same investigation performed on SPCE modified by drop-casting led to the formation of AuNPs aggregates mainly located at the outer edges of the carbon electrode and a scarce presence of nanoparticles on the electrode surface, see Figure S4. The images were obtained with an electron beam generated using two different electron acceleration voltages (15 and 5 kV), and the acquisition was carried out using a detector for secondary electrons in the two modes LEI (lower secondary electron detector) and SEI (secondary electron detector). As can be noticed, the electrochemical deposition of AuNPs is a very effective approach leading to a homogeneous and uniform distribution of AuNPs with dimensions between 200 and 400 nm over the entire surface of the SPCE.

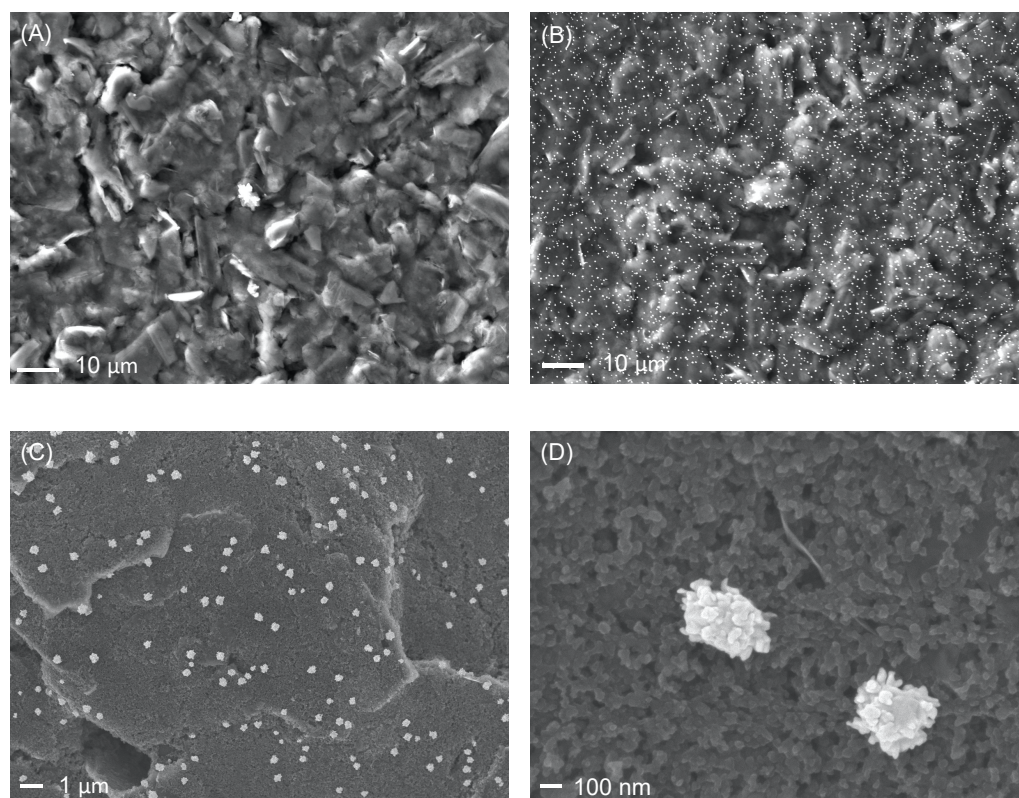


**Figure 4.** FE-SEM images of unmodified SPCE (A), AuNPs-modified SPCE (B), AuNPs-modified SPCE at different magnifications (C,D).

### 3.3. Electrochemical Characterization of the Biosensor

Based on the results reported in Sections 3.1 and 3.2, the subsequent experimental work has been performed on the SPCE modified with the electrogenerated AuNPs. In order to verify the effectiveness of the SPCE modification procedure, a surface characterization was performed at the end of each modification step using EIS measurements. Figure 5 shows the relevant Nyquist plots confirming the correct surface modifications. In fact, the resistance to charge transfer increase progressively from the deposition of streptavidin ( $R_{ct} = 384.82 \Omega$ ) to BSA-sorbitol ( $R_{ct} = 403.68 \Omega$ ) and Gli4-T ( $R_{ct} = 456.59 \Omega$ ). In addition, after biotin immobilization ( $R_{ct} = 469.33 \Omega$ ), there were no substantial changes indicating that the surface was already properly blocked and ready for subsequent measurements. Impedance behavior recorded at SPCE is due to an increasing difficulty for the electroactive pair ferrocyanide/ferricyanide to reach the electrode surface and to an increasingly resistive electrode surface. As expected, this trend can be correlated to the correct adsorption of biomolecules during the modification steps. Finally, after the incubation with PWG-Gliadin  $0.5 \text{ mg L}^{-1}$ , thanks to steric hindrance, the value of  $R_{ct}$  increased substantially ( $R_{ct} = 586.61 \Omega$ ).

### 3.4. Gliadin Quantification by Label-Free Biosensor

The biosensor was calibrated by analyzing solutions with a known concentration of PWG-Gliadin, which is a fraction of gluten (approximately 50%) commonly used as an analytical target. The signals obtained for each concentration of PWG-Gliadin have been subtracted from the blank to compare the data obtained on different days. Figure 6 shows the Nyquist plots recorded for increasing concentrations of PWG-Gliadin (0, 0.2, 0.4, 0.6, 0.8,  $1 \text{ mg L}^{-1}$ ) and the relative calibration curve obtained from three different repetitions.

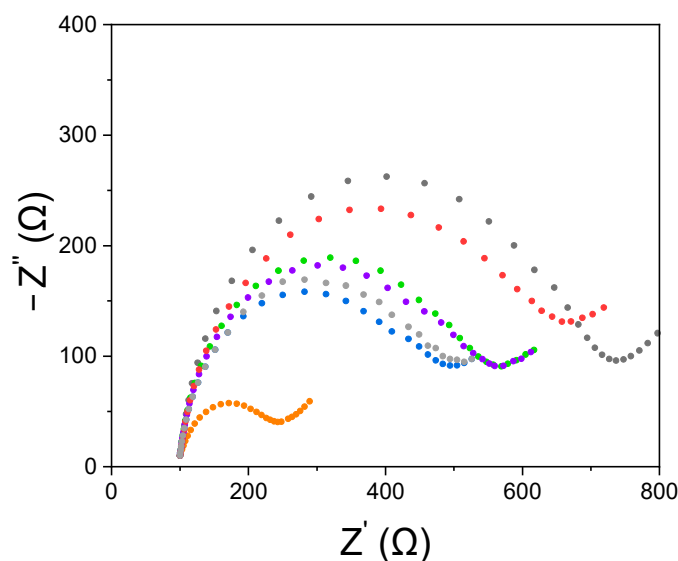


**Figure 5.** Nyquist plots recorded on SPCE using the redox probe  $[\text{Fe}(\text{CN})_6]^{4-}/[\text{Fe}(\text{CN})_6]^{3-}$  2 mM each, KCl 3 mM in PBS: unmodified (black,  $R_{\text{ct}} = 614.44 \Omega$ ), modified with electrogenerated AuNPs (orange,  $R_{\text{ct}} = 172.95 \Omega$ ), modified with streptavidin (blue,  $R_{\text{ct}} = 384.82 \Omega$ ), after 30 min of BSA-sorbitol (grey,  $R_{\text{ct}} = 403.68 \Omega$ ) after 30 min of Gli4-T (purple,  $R_{\text{ct}} = 456.59 \Omega$ ), after 10 min of biotin (green,  $R_{\text{ct}} = 469.33 \Omega$ ) and after 30 min of PWG-Gliadin  $0.5 \text{ mg L}^{-1}$  (red,  $R_{\text{ct}} = 586.61 \Omega$ ).

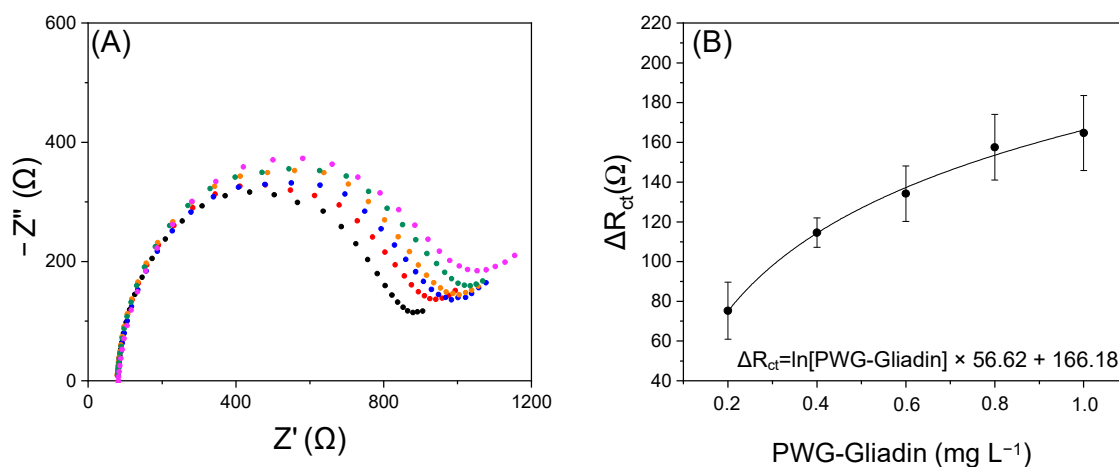


**Figure 6.** (A) Nyquist plots recorded for increasing concentrations of PWG-Gliadin (0, 0.2, 0.4, 0.6, 0.8, 1  $\text{mg L}^{-1}$ ), (B) Calibration curve used for the determination of the gliadin content in real samples. The error bars correspond to the standard deviation evaluated on a minimum of three measurements at each point.

The calibration fitted the Levenberg–Marquardt function with a correlation of 0.994. The limit of detection (LOD), calculated as three times the standard deviation of the blank signal divided by the slope calculated for the linear dynamic range, and the limit of quantification (LOQ), estimated by multiplying the LOD by 3.3, were found to be 0.05 and 0.16  $\text{mg L}^{-1}$  of gliadin (corresponding to 0.1 and 0.32  $\text{mg L}^{-1}$  of gluten respectively). Stability tests show that the sensor response does not change significantly during 5 days, see Figure S5. Finally, as can be seen from Table 1, the proposed sensor successfully competes with those reported in the literature and present on the market so far.

**Table 1.** Comparison of the analytical performance of different label-free approaches for gluten detection.

Method	Recognition Element	LOD/mg L <sup>-1</sup> (Gluten)	Linear Range/mg L <sup>-1</sup> (Gluten)	Ref.
Label-free (impedance)	aptamer	5	-	[35]
Label-free (impedance)	antibody	5	5–20	[36]
Label-free (impedance)	antibody	14	0–20	[40]
Label-free (impedance)	aptamer	0.1	0.4–2	This work

### 3.5. Real Samples Analysis

The gluten content of two gluten-free beers and one gluten-free soy sauce were tested. In these samples, gluten is present in the hydrolyzed form and, therefore, cannot be determined with the classic sandwich approaches. The samples were also analyzed after their enrichment with a known quantity of PWG-Gliadin. All samples were diluted 1/20 and analyzed following the procedure previously described for PWG-Gliadin standards. Table 2 reports gluten contents determined in real samples, in enriched samples, and the related recovery (%). Some representative raw Nyquist plots of real samples and spiked samples are reported in Figure S6.

**Table 2.** Gluten quantification in different food matrices with the label-free aptasensor.

Sample	Expected Gluten Concentration (mg L <sup>-1</sup> ) *	Gluten Concentration (mg L <sup>-1</sup> ) **	Recovery (%) ***
Beer 1	<20	12.96 ± 1.68	\
Beer 1 (spiked with 5 mg L <sup>-1</sup> )	16.66	16.80 ± 2.21	101
Beer 2	<20	18.38 ± 1.04	\
Beer 2 (spiked with 10 mg L <sup>-1</sup> )	26.54	27.81 ± 3.49	105
Soy sauce	<20	8.72 ± 0.27	\
Soy sauce (spiked with 10 mg L <sup>-1</sup> )	17.85	16.59 ± 2.02	93

\* The expected concentration in the added samples was calculated considering the initial concentration, the addition of PWG-Gliadin multiplied by two and the dilution attributable to the addition itself. \*\* Average of three repetitions. \*\*\* Obtained as the ratio between the gluten concentration determined and that expected in the spiked samples.

As can be seen from Table 2, in all three analyzed samples, the gluten content is below the limit of 20 mg L<sup>-1</sup>. Furthermore, the recoveries calculated for the spiked samples are close to 100%, confirming the aptasensor's ability to provide accurate and reproducible data in these matrices.

## 4. Conclusions

In this work, we have proposed a simple label-free and easy-to-use biosensor. The impedimetric aptasensor developed was built on disposable graphite screen-printed electrodes modified with gold nanoparticles and the truncated aptamer Gli4-T. The modification of the biosensor surface was carried out by the electrogeneration of AuNPs using tetrachloroauric acid. A good relationship between the R<sub>ct</sub> values and PWG-Gliadin concentration was found in the range between 0.1–1 mg L<sup>-1</sup> of gliadin (corresponding to 0.2–2 mg L<sup>-1</sup> of

gluten) with a limit of detection of  $0.05 \text{ mg L}^{-1}$  of gliadin (corresponding to  $0.1 \text{ mg L}^{-1}$  of gluten). The label-free assay was also applied for the determination of spiked samples of food bought in local supermarkets. These results can be very important for the improvement of gluten quantification, especially in those matrices where gluten is present in the hydrolyzed form. Finally, our study demonstrates that the use of gold particles is a valid strategy to increase the sensitivity of label-free assays.

**Supplementary Materials:** The following supporting information can be downloaded at: <https://www.mdpi.com/article/10.3390/nano12060987/s1>, Figure S1: Characterization of the electrode surface with EIS after the electrodeposition of AuNPs at different potentials (0.18 V, 0.4 V and 0.6 V); Figure S2: Trend of the charge (C) spent during the electrogeneration of AuNPs at 0.18 V at different times (10, 20, 30, 40, 50 and 60 s); Figure S3: Characterization of the electrode surface with EIS after the electrodeposition of AuNPs at different times (10, 20, 30, 40, 50 and 60 s); Figure S4: (A) Enlargement of the surface of the SPCE where most of the drop-casted nanoparticles form aggregates. (B) FE-SEM images of the carbon surface obtained by drop-casting of AuNPs; Figure S5: Biosensor stability experiment:  $\Delta R_{ct}$  ( $\Omega$ ) values recorded in different days for a solution containing  $0.6 \text{ mg L}^{-1}$  of PWG-Gliadin; Figure S6: Nyquist plots recorded for real samples and their corresponding spiked sample (A) Beer 1, (B) Beer 2 and (C) Soy sauce.

**Author Contributions:** Conceptualization, R.S. and R.T.; methodology, R.S., I.Z. and C.G.; investigation, R.S. and I.Z.; resources, R.T.; data curation, R.S. and I.Z.; writing—original draft preparation, R.S. and R.T.; writing—review and editing, N.D. and C.G.; visualization, R.S.; supervision, R.T. and N.D. All authors have read and agreed to the published version of the manuscript.

**Funding:** This research received no external funding.

**Institutional Review Board Statement:** Not applicable.

**Data Availability Statement:** The data presented in this study are available on request from the corresponding author.

**Acknowledgments:** We thank Lorenzo Fedrizzi and Ruben Offoiach, of the Polytechnic Department of Engineering and Architecture, of the University of Udine, for the FE-SEM measurements.

**Conflicts of Interest:** The authors declare no conflict of interest.

## References

1. Pan, M.; Gu, Y.; Yun, Y.; Li, M.; Jin, X.; Wang, S. Nanomaterials for electrochemical immunosensing. *Sensors* **2017**, *17*, 1041. [[CrossRef](#)] [[PubMed](#)]
2. Bobrinetskiy, I.; Radovic, M.; Rizzotto, F.; Vizzini, P.; Jaric, S.; Pavlovic, Z.; Radonic, V.; Nikolic, M.; Vidic, J. Advances in nanomaterials-based electrochemical biosensors for foodborne pathogen detection. *Nanomaterials* **2021**, *11*, 2700. [[CrossRef](#)] [[PubMed](#)]
3. Cavalcante, F.T.T.; de Falcão, I.R.A.; da Souza, J.E.S.; Rocha, T.G.; de Sousa, I.G.; Cavalcante, A.L.G.; de Oliveira, A.L.B.; de Sousa, M.C.M.; dos Santos, J.C.S. Designing of nanomaterials-based enzymatic biosensors: Synthesis, properties, and applications. *Electrochem* **2021**, *2*, 149–184. [[CrossRef](#)]
4. Su, S.; Kang, P. Systemic review of biodegradable nanomaterials in nanomedicine. *Nanomaterials* **2020**, *10*, 656. [[CrossRef](#)] [[PubMed](#)]
5. Fuentes-Chust, C.; Parolo, C.; Rosati, G.; Rivas, L.; Perez-Toralla, K.; Simon, S.; Lecuona, I.; Junot, C.; Trebicka, J.; Merkoçi, A. The microbiome meets nanotechnology: Opportunities and challenges in developing new diagnostic devices. *Adv. Mater.* **2021**, *33*, 2006104. [[CrossRef](#)]
6. Share, K.; Westover, A.; Li, M.; Pint, C. Surface engineering of nanomaterials for improved energy storage—A review. *Chem. Eng. Sci.* **2016**, *154*, 3–19. [[CrossRef](#)]
7. Saleem, H.; Zaidi, S. Recent developments in the application of nanomaterials in agroecosystems. *Nanomaterials* **2020**, *10*, 2411. [[CrossRef](#)] [[PubMed](#)]
8. Yang, J.; Hou, B.; Wang, J.; Tian, B.; Bi, J.; Wang, N.; Li, X.; Huang, X. Nanomaterials for the removal of heavy metals from wastewater. *Nanomaterials* **2019**, *9*, 424. [[CrossRef](#)] [[PubMed](#)]
9. Tonelli, D.; Scavetta, E.; Gualandi, I. Electrochemical deposition of nanomaterials for electrochemical sensing. *Sensors* **2019**, *19*, 1186. [[CrossRef](#)] [[PubMed](#)]
10. Antuña-Jiménez, D.; González-García, M.B.; Hernández-Santos, D.; Fanjul-Bolado, P. Screen-printed electrodes modified with metal nanoparticles for small molecule sensing. *Biosensors* **2020**, *10*, 9. [[CrossRef](#)] [[PubMed](#)]

11. Alam, S.; Augustine, S.; Narayan, T.; Luong, J.H.T.; Malhotra, B.D.; Khare, S.K. A chemosensor based on gold nanoparticles and dithiothreitol (DTT) for acrylamide electroanalysis. *Nanomaterials* **2021**, *11*, 2610. [[CrossRef](#)] [[PubMed](#)]
12. Yu, L.; Li, N. Noble metal nanoparticles-based colorimetric biosensor for visual quantification: A mini review. *Chemosensors* **2019**, *7*, 53. [[CrossRef](#)]
13. Qing, Z.; Bai, A.; Xing, S.; Zou, Z.; He, X.; Wang, K.; Yang, R. Progress in biosensor based on DNA-templated copper nanoparticles. *Biosens. Bioelectron.* **2019**, *137*, 96–109. [[CrossRef](#)] [[PubMed](#)]
14. Sun, Y.; Ma, C.; Wu, M.; Jia, C.; Feng, S.; Zhao, J.; Liang, L. Sensitivity of photoelectrochemical aptasensor using spiral nanorods for detecting antibiotic levels in experimental and real samples. *Talanta* **2022**, *237*, 122930. [[CrossRef](#)] [[PubMed](#)]
15. Ahmadi, S.; Hojjatoleslami, M.; Kiani, H.; Molavi, H. Monitoring of aflatoxin M1 in milk using a novel electrochemical aptasensor based on reduced graphene oxide and gold nanoparticles. *Food Chem.* **2022**, *373*, 131321. [[CrossRef](#)]
16. Cao, X.; Ye, Y.; Liu, S. Gold nanoparticle-based signal amplification for biosensing. *Anal. Biochem.* **2011**, *417*, 1–16. [[CrossRef](#)] [[PubMed](#)]
17. Pingarrón, J.M.; Yáñez-Sedeño, P.; González-Cortés, A. Gold nanoparticle-based electrochemical biosensors. *Electrochim. Acta* **2008**, *53*, 5848–5866. [[CrossRef](#)]
18. Xiao, T.; Huang, J.; Wang, D.; Meng, T.; Yang, X. Au and Au-based nanomaterials: Synthesis and recent progress in electrochemical sensor applications. *Talanta* **2020**, *206*, 120210. [[CrossRef](#)] [[PubMed](#)]
19. Fang, X.; Bai, L.; Han, X.; Wang, J.; Shi, A.; Zhang, Y. Ultra-sensitive biosensor for K-Ras gene detection using enzyme capped gold nanoparticles conjugates for signal amplification. *Anal. Biochem.* **2014**, *460*, 47–53. [[CrossRef](#)]
20. Lin, C.-Y.; Nhat Nguyen, U.T.; Hsieh, H.-Y.; Tahara, H.; Chang, Y.-S.; Wang, B.-Y.; Gu, B.-C.; Dai, Y.-H.; Wu, C.-C.; Tsai, I.-J.; et al. Peptide-based electrochemical sensor with nanogold enhancement for detecting rheumatoid arthritis. *Talanta* **2022**, *236*, 122886. [[CrossRef](#)] [[PubMed](#)]
21. Neethirajan, S.; Weng, X.; Tah, A.; Cordero, J.O.; Ragavan, K.V. Nano-biosensor platforms for detecting food allergens—New trends. *Sens. Bio-Sens. Res.* **2018**, *18*, 13–30. [[CrossRef](#)]
22. Aquino, A.; Conte-Junior, C.A. A systematic review of food allergy: Nanobiosensor and food allergen detection. *Biosensors* **2020**, *10*, 194. [[CrossRef](#)]
23. Alves, R.C.; Barroso, M.F.; González-García, M.B.; Oliveira, M.B.P.P.; Delerue-Matos, C. New trends in food allergens detection: Toward biosensing strategies. *Crit. Rev. Food Sci. Nutr.* **2016**, *56*, 2304–2319. [[CrossRef](#)] [[PubMed](#)]
24. Wieser, H.; Koehler, P. The biochemical basis of celiac disease. *Cereal Chem. J.* **2008**, *85*, 1–13. [[CrossRef](#)]
25. Uche-Anyia, E.; Lebowohl, B. Celiac disease: Clinical update. *Curr. Opin. Gastroenterol.* **2021**, *37*, 619–624. [[CrossRef](#)]
26. Prandi, B.; Bencivenni, M.; Faccini, A.; Tedeschi, T.; Dossena, A.; Marchelli, R.; Galaverna, G.; Sforza, S. Composition of peptide mixtures derived from simulated gastrointestinal digestion of prolamins from different wheat varieties. *J. Cereal Sci.* **2012**, *56*, 223–231. [[CrossRef](#)]
27. Mamone, G.; Ferranti, P.; Rossi, M.; Roepstorff, P.; Fierro, O.; Malorni, A.; Addeo, F. Identification of a peptide from  $\alpha$ -Gliadin resistant to digestive enzymes: Implications for celiac disease. *J. Chromatogr. B* **2007**, *855*, 236–241. [[CrossRef](#)] [[PubMed](#)]
28. De Re, V.; Caggiari, L.; Tabuso, M.; Cannizzaro, R. The versatile role of gliadin peptides in celiac disease. *Clin. Biochem.* **2013**, *46*, 552–560. [[CrossRef](#)]
29. Colgrave, M.L.; Goswami, H.; Blundell, M.; Howitt, C.A.; Tanner, G.J. Using mass spectrometry to detect hydrolysed gluten in beer that is responsible for false negatives by ELISA. *J. Chromatogr. A* **2014**, *1370*, 105–114. [[CrossRef](#)] [[PubMed](#)]
30. Morón, B.; Cebolla, A.; Manyani, H.; Alvarez-Maqueda, M.; Megías, M.; Thomas, M.D.C.; López, M.C.; Sousa, C. Sensitive detection of cereal fractions that are toxic to celiac disease patients by using monoclonal antibodies to a main immunogenic wheat peptide. *Am. J. Clin. Nutr.* **2008**, *87*, 405–414. [[CrossRef](#)]
31. Amaya-González, S.; de-los-Santos-Álvarez, N.; Miranda-Ordieres, A.J.; Lobo-Castañón, M.J. Aptamer binding to celiac disease-triggering hydrophobic proteins: A sensitive gluten detection approach. *Anal. Chem.* **2014**, *86*, 2733–2739. [[CrossRef](#)]
32. Amaya-González, S.; López-López, L.; Miranda-Castro, R.; de-los-Santos-Álvarez, N.; Miranda-Ordieres, A.J.; Lobo-Castañón, M.J. Affinity of aptamers binding 33-Mer gliadin peptide and gluten proteins: Influence of immobilization and labeling tags. *Anal. Chim. Acta* **2015**, *873*, 63–70. [[CrossRef](#)] [[PubMed](#)]
33. Svirgelj, R.; Dossi, N.; Pizzolato, S.; Toniolo, R.; Miranda-Castro, R.; de-los-Santos-Álvarez, N.; Lobo-Castañón, M.J. Truncated aptamers as selective receptors in a gluten sensor supporting direct measurement in a deep eutectic solvent. *Biosens. Bioelectron.* **2020**, *165*, 112339. [[CrossRef](#)]
34. Svirgelj, R.; Dossi, N.; Grazioli, C.; Toniolo, R. Paper-based aptamer-antibody biosensor for gluten detection in a deep eutectic solvent (DES). *Anal. Bioanal. Chem.* **2021**, 1–8. [[CrossRef](#)] [[PubMed](#)]
35. Malvano, F.; Albanese, D.; Pilloton, R.; Matteo, M.D. A New label-free impedimetric aptasensor for gluten detection. *Food Control* **2017**, *79*, 200–206. [[CrossRef](#)]
36. Bottari, F.; Moretto, L.M.; Ugo, P. Impedimetric sensing of the immuno-enzymatic reaction of gliadin with a collagen-modified electrode. *Electrochem. Commun.* **2018**, *97*, 51–55. [[CrossRef](#)]
37. Lopes, P.; Costa-Rama, E.; Beirão, I.; Nouws, H.P.A.; Santos-Silva, A.; Delerue-Matos, C. Disposable electrochemical immunosensor for analysis of cystatin C, a CKD biomarker. *Talanta* **2019**, *201*, 211–216. [[CrossRef](#)]

38. Alves, R.C.; Pimentel, F.B.; Nouws, H.P.A.; Correr, W.; González-García, M.B.; Oliveira, M.B.P.P.; Delerue-Matos, C. Detection of the peanut allergen ara h 6 in foodstuffs using a voltammetric biosensing approach. *Anal. Bioanal. Chem.* **2015**, *407*, 7157–7163. [[CrossRef](#)]
39. Liu, J.; Lu, Y. Preparation of aptamer-linked gold nanoparticle purple aggregates for colorimetric sensing of analytes. *Nat. Protoc.* **2006**, *1*, 246–252. [[CrossRef](#)] [[PubMed](#)]
40. Dumitriu, C.; Constantinescu, A.; Pirvu, C. Functionalized TiO<sub>2</sub> nanotube platform for gliadin electroanalysis. *Crystals* **2020**, *11*, 22. [[CrossRef](#)]